IEEE Access
Multidisciplinary | Rapid Review | Open Access Journal

Received July 21, 2020, accepted September 2, 2020, date of publication September 14, 2020, date of current version September 30, 2020.

Digital Object Identifier 10.1109/ACCESS.2020.3024020

An Innovative Multifunctional Buoy Design for Monitoring Continuous Environmental Dynamics at Tianjin Port

HAO ZHANG, DIANJUN ZHANG, AND ANMIN ZHANG
School of Marine Science and Technology, Tianjin University, Tianjin 300072, China
Corresponding author: Dianjun Zhang (dj.zhang@tju.edu.cn)

This work was supported by the National Key Research and Development Program of China under Grant 2018YFC1407400.

ABSTRACT The Tianjin port plays a relevant role in driving both ship navigation and the weather and climate of the area. To better understand the underlying peculiarities of this area, several in-service coastal ocean system and facilities have been constructed, at present, the whole coastal ocean systems at Tianjin port have been improved, however, they cannot meet the safety requirements of traffic management and navigational safety. Marine buoys have the unreplaceable advantages of long-term, real-time, reliable capabilities and trivial environmental restrictions to monitor the marine dynamics. Here an innovative multifunctional buoy prototype is proposed to continuously measure meteorological and oceanographic parameters at a high spatial and temporal resolution, which can ensure navigation safety at Tianjin Port. Solar panels and battery module are personalized to ensure electric supply to the buoy system. An independent ARM (Advanced RISC Machine)-based module is affiliated to maintain the stability of the data acquisition and communication module. Buoy platform based on Beidou difference is proved to be an effective approach for the tide measurement. Additionally, a web-designed software for data acquisition is integrated for the visualization purpose. Finally, in-field recording test at Tianjin port will be performed to verify effectiveness of our system on monitoring environment dynamics. It turns out that our buoy prototype functions as a reliable and energy favorable electrical device and shed light on the development of effective measurement instruments working under unpredictable and harsh marine environment.

INDEX TERMS Buoy monitoring system, power supply, sensor, port environmental dynamics.

I. INTRODUCTION

The coastal ocean is one important component of the earth system where land, water, air, and people meet together. However the coastal ocean condition becomes fragile due to the emerging populations, businesses, and infrastructure are increasing along coastlines [1]. Long-term and ad-hoc atmospheric and oceanographic monitoring in the coastal ocean is a well-recognized topic to the scientific community involved in the study of the atmosphere, the ocean, and their interactions. Long-term ocean data such as the temperature, salinity, ocean current and oceanographic meteorology are crucial for the air-sea exchange processes, weather phenomena, and possible climate changes [2]. The real-time data can also be exploited for local forecasts to dealing with marine research such as analysis of ocean circulation, internal solitary wave, upwelling and other phenomena, especially the synchronous observation data of sea surface, water body and seabed, which can reveal some special ocean mechanisms. Therefore, it is of great significance to obtain long-term and continuous monitoring data for operational and research activities like physical oceanography research, marine development and protection as well as natural hazards alarm [3].

In general the presently available ways to obtain marine data include [1], measured by satellite-mounted, in situ, ship or buoy. Satellite products could offer data with a large-scale coverage, but satellite data is discontinuous in time need a validation effort to characterize the overall accuracy of the derived datasets [4], [5]. Ship could provide a valid support for suitable data collection, however it is limited in time and space and exists difficulties arising from adverse sea conditions, and they are obviously expensive. Thus when consider a specific zone, the permanent custom-made facilities like drifting buoys [6], profiling floats (e.g., ARGO), and networks of moored buoys [7] are capable of providing in situ long-term marine data collection.

The associate editor coordinating the review of this manuscript and approving it for publication was Yanli Xu.

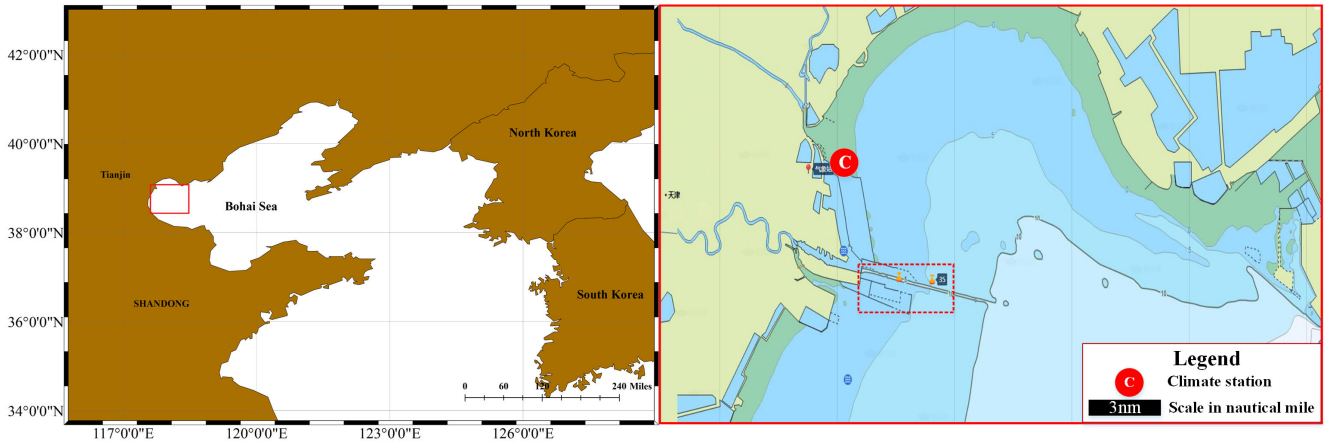

FIGURE 1. The Bohai Sea region (left panel) and the area of interest (right panel).

Much efforts have been devoted to develop ocean monitoring buoys for marine data collection and environmental protection. Previously, CMS-OCG (College of Marine Science, Ocean Circulation Group) buoys along with other platforms have been developed to provide meteorological and oceanographic observations in support of a variety of coastal ocean programs [8]. Data such as currents, temperature, and conductivity could be gathered by the Geostationary Operational Environmental Satellite (GOES) system maintained by National Oceanic and Atmospheric Administration (NOAA). The Gulf of Maine Ocean Observing System (GoMOOS) has initiated as a prototype for regional sustainable ocean observing systems in energetic environments [9]. The critical component of GoMOOS is the real-time buoy array deployed in a region with very little history of successful year-round scientific surface mooring deployments. A compact wave and ocean data buoy system, called the COLOS (Compact Ocean and Littoral Observing System) buoy system, was designed by the NOAA's (National Oceanic and Atmospheric Administration) National Data Buoy Center (NDBC) to support its expanding networks and ocean measurement capabilities [10]. Nagai *et al.* introduced a basic design of GPS buoy with multi-objective data processing system via numerical filtering analysis in 2009, and deployed the blueprints of the GPS buoy network in Japan [11]. Venkatesan *et al.* have paid their attention to reliable performance of offshore moored buoys on cyclone monitoring, reliability modeling and maintenance strategies [7]. Sara *et al* have collected all the time series by the W1-M3A off-shore observatory moored at 40 nautical miles away from the Genoa coasts, in the center of Ligurian basin on a deep sea bed (1250m) and demonstrate the multidisciplinary nature of the system and its monitoring capability on the physical processes involving both the atmosphere and ocean [12]. Elisa *et al* have described the Oceanographic Data Acquisition System (ODAS) Italia 1 buoy's historical background and discussed the scientific results that have been obtained exploiting the data from the system [2]. Weisberg *et al* have created a comprehensive coastal ocean observing and modeling system for the west coast of Florida based on the lessons learned through their sustained long-term coastal ocean observing and modeling efforts over the last two decades [13]. Wang Juncheng *et al* have introduced technology development and application of marine data buoy in China [14], expected the development trend of marine data buoy and buoy monitoring network.

The Bohai Sea is a marginal sea approximately 78,000 km^2 in area on the east coast of mainland China. The Bohai Sea is a medium-sized gulf, enclosed by four provinces from three different regions of China [15]. Tianjin Port is on the coast of Tianjin Municipality, on the coast between the estuaries of the Haihe to the south and the New Yongding River to the north. To the west, the port borders the city of Tanggu (now the Urban Core of the Binhai New Area) and the TEDA. To the east, the port opens up to the Bohai Bay. (Fig. 1). The tide in Tianjin Port belongs to irregular semi-diurnal tide. The annual average high tide level is 3.74M, the annual average low tide level is 1.34m, and the average sea level is 2.56M. The annual ice age in Bohai Bay lasts for three months (from the first ten days of December to the beginning of March of the following year), and the ice condition reach worst from the middle of January to the middle of February. Tianjin Port is the largest man-made in Northern China and the main maritime gateway to Beijing. Tianjin Port divides into nine areas including the three core areas of Beijiang, Nanjiang, and Dongjiang around the Xingang fairway, the Haihe area along the river; the Beitang Port Area around the Beitangkou estuary; the Dagukou Port Area in the estuary of the Haihe River; and three areas under construction (Hanggu, Gaoshaling, Nangang). The main shipping channel is 39.5km long with dredging to a depth of -19.5m and a bottom width of 420m, with making it capable of handling two-way 250000 DWT traffic, and to accept 300000 DWT ships at high tide. There are two service channels(100m wide and 9m deep) at each side of the main channel which allow ships under 10000 DWT to transit without interference the big ships [16]. Significant environmental conditions and important geographical location make Bohai Sea an interesting research site for scholars, and complex environmental

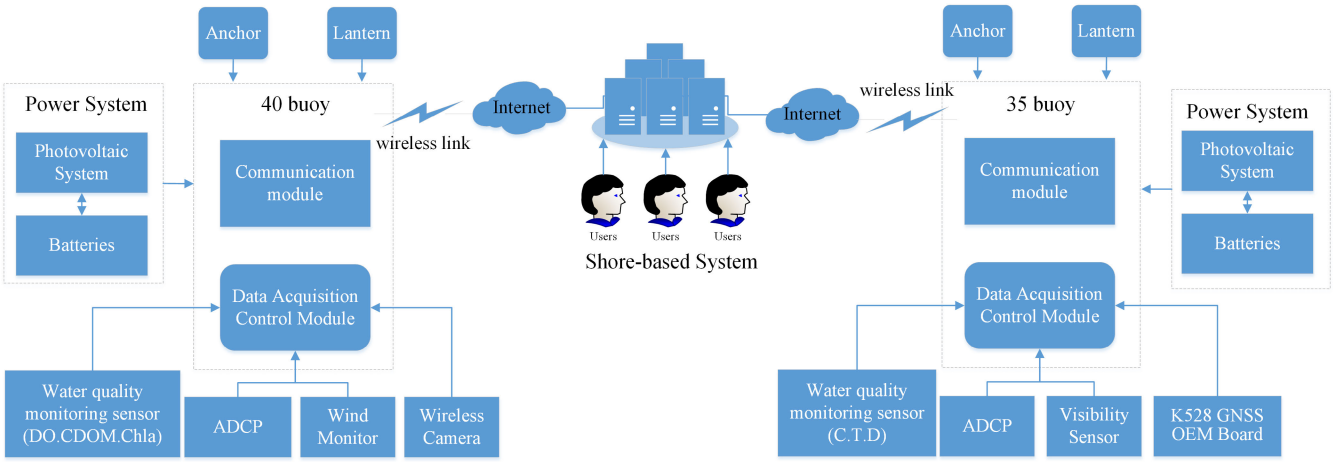

FIGURE 2. The architecture of the monitoring system.

conditions also put forward higher requirements for coastal ocean monitoring.

Recently, Tianjin Port have been devoted to aids to navigation (AtoN) system and coastal ocean monitoring system. However, with the increasing vessel traffic at Tianjin Port, the existing monitoring system of water environment cannot meet the safety navigation requirement. It is required to upgrade water environment monitoring equipment according to hydrological, meteorological, visibility and other environmental data collection.

In this work, we have designed an innovative buoy for continuously monitoring environmental dynamics at Tianjin port. A monitoring prototype assembled with many kinds of sensors is proposed to acquire flow and wave information at Tianjin port and fulfil the requirement of long-term observation and real-time transmission for hydrometeorology information on the sea surface. We initially put forward to the detailed design of buoy, power supply, sensor equipment, communication and shore-based environmental monitoring system. A tide measurement method based on Beidou difference is also implemented into the buoy platform. Then we have conducted systematic field test to validate the effectiveness the buoy platform on the real-time monitoring on the marine dynamics. It can be estimated that our proposed platform could boost the development of effective measurement instruments working under complex marine environment.

II. MONITORING SYSTEM

The architecture of the monitoring system is shown in Fig. 2. In general, the monitoring platform is composed of a pair of buoys named as No.40 and No.35 buoy that has similar technical specifications except for mooring, buoy hull and lantern (Fig. 3a). No.40 buoy is integrated with water quality meter, ADCP (Acoustic Doppler Current Profiler) and wind monitor sensors (Fig. 3a), whereas No.35 buoy is mounted with water quality meter, tidal observation system, ADCP and visibility meter (Fig. 3b). Each buoy is equipped with control module and transmission module as well. The control module can realize the cooperative operation and the remote configuration of the sensing module. The transmission module establishes the communication link between the monitoring platform and the shore-based control center to realize the real-time monitoring and data analysis of the water environment. Detailed designs of each module will be discussed in the following sections.

A. BUOY DESIGN

Ultra-high molecular weight polyethylene (UHMWPE) is chosen for the buoy hull to arm with high resistance of impact and corrosion, which could be used under $-70°C$ to $80°C$. The cylindrical shape of the buoy hull has enough interior room for technical equipment and allow easy accessibility for maintenance (Fig. 3a). A cabin made of fiber reinforced polymer/plastic (FRP) is embedded in the middle of the buoy hull (Fig. 3b). Two instrument wells on both sides of the cabin accommodate water quality monitoring instruments (Fig. 3d), and have a fixed bracket for anchoring the monitoring instruments.

There is an outer flange on the upper part of the instrument compartment, and a groove is set on the flange to place the O-ring, and the stainless-steel bolt is used to fix the round FRP hatch cover. The upper part of the instrument cabin is a cylinder with a diameter of 600 mm, and the middle part is flattened to be a flat circle with a width of 400 mm. The space inside the instrument cabin is no less than $600\text{mm} * 400\text{mm} * 500\text{mm}$. The side plate and bottom plate of the flat circle is used to install instruments. The instrument cable shall be penetrated into the cabin from the bottom to the top, and the cable outside the instrument cabin is extended by the embedded threading pipe in the buoy hull, and the outer side is covered by the arc cover plate that has been cut off to prevent the direct impact from the wave and the atmospheric exposure.

Fig. 4 shows the technical architecture of instrument wells. The diameter of instrument wells is 280mm to meet the installing requirements of water quality meter, ADCP, etc. A cable tube is put in the instrument well toward the instrument cabin. The upper part of the instrument well has an

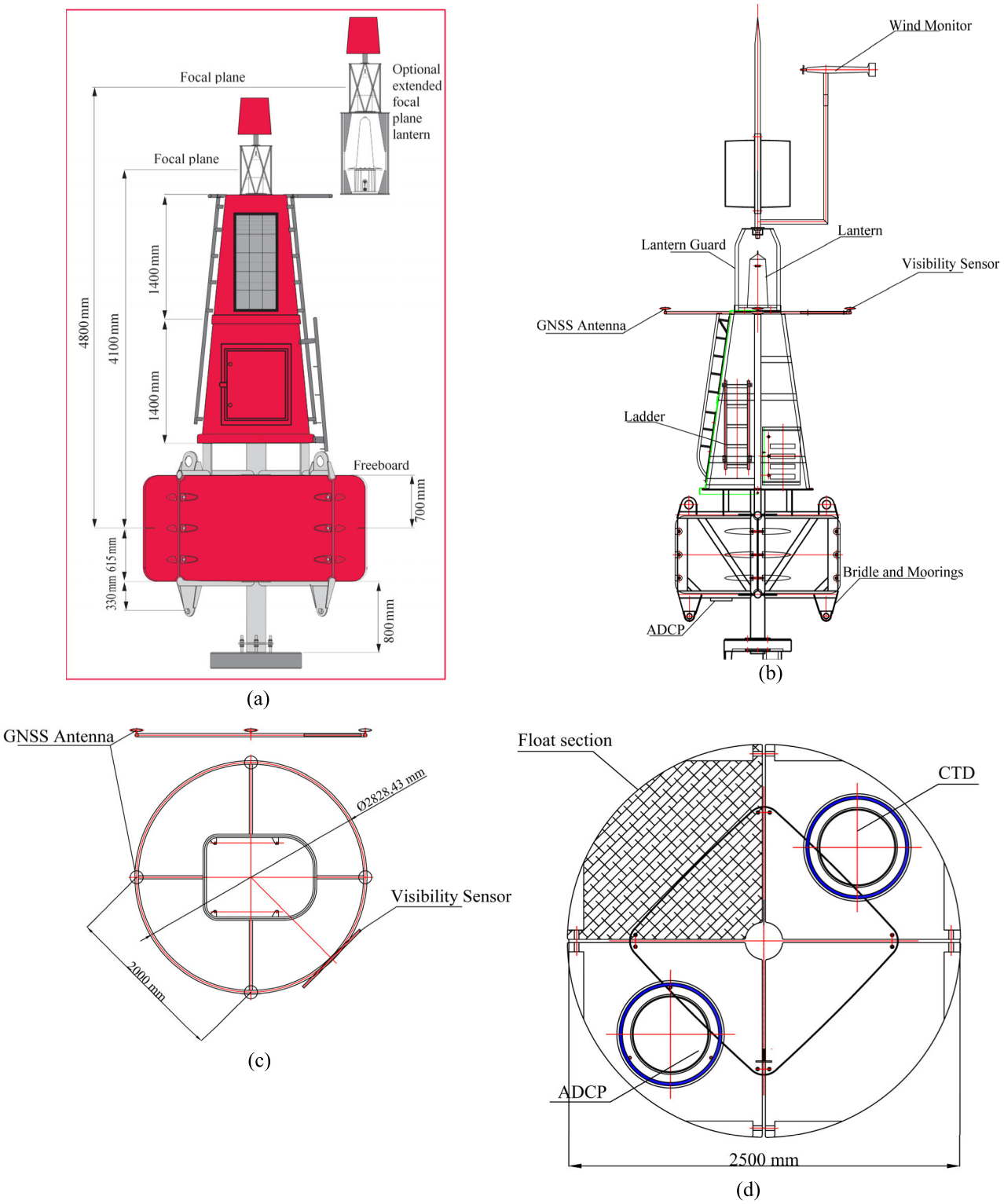

FIGURE 3. Schematic diagram of the buoy hull. (a) The render side view of No.40 buoy; (b) The side view of No.35 buoy; (c, d) The top view of the buoy hull.

anti-theft well cover. An instrument fixing bracket is set inside the instrument well, and a hoop is used to fix sensor units to reduce the risk of instrument damage. The bottom of the instrument well protrudes from the bottom of the buoy hull and the protrusion is arranged along the inner side under the well to prevent the instrument and the bracket from falling off accidentally.

The top of the upper buoy bracket has a retainer where a beacon light and anemometer bracket could be installed (Fig. 3c). The middle part of the bracket has a mounting

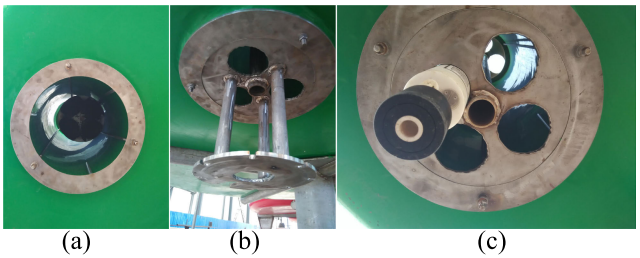

FIGURE 4. Technical architecture of instrument wells. (a) The physical view of instrument wells; (b) The fixing bracket for ADCP; (c) The fixing bracket for water quality monitoring sensor.

TABLE 1. Some detailed technical parameters of buoy system.

Skeleton Material	316L
Construction	UHMWPE
Foam Filling	polyurethane foam
Diameter	2500mm
Thickness	12mm
Weight	2.5T
Draft	1400mm
Freeboard	700mm
Nominal Focal Plane Height	4100mm
Visual Area	$5m^2$
Submergence	24.5KN
Maximum Mooring Load	2800kg
Maximum Current	7knots

frame of solar panel and a cable transfer sealing box. The solar array installed on the bracket is consisted of four 1068mm × 806mm modules, inclined at 75° to ensure better lighting efficiency [17]. The solar panel junction box is sealed with silica gel that ensure the long-term function in the humid environment. A glass fiber reinforced plastic back plate is installed between the solar panel and the mounting bracket which can reduce the electrochemical corrosion of metal materials and protect the solar panel from the erosion of splashing waves.

All connecting parts of the buoy hull were connected by 316L stainless-steel bolts, the bracket was treated with special anti-rust treatment, which could effectively extend the service life. The buoy hull combined flexibility with high elasticity and hardness, which could absorb the impact energy and return to its original shape after being hit by an external force. Some detailed technical parameters as shown in Table 1.

B. DESIGN OF POWER SUPPLY

When configuring solar power system, it is necessary to meet the requirement of the load and reliability under safety conditions. Fig. 5 shows the mean daily shortwave radiation of each month in the region ($117°43'12''E$, $39°N$) from 2005 to 2010 [18]. To guarantee ordinary work of the system at different seasons, solar panels, batteries with large capacity as well as power controller should be included as shown in Fig. 6. Solar panels are used as the primary power source for continuous power supply for the buoy system. The battery module, as supplementary power supply, is chosen from lithium

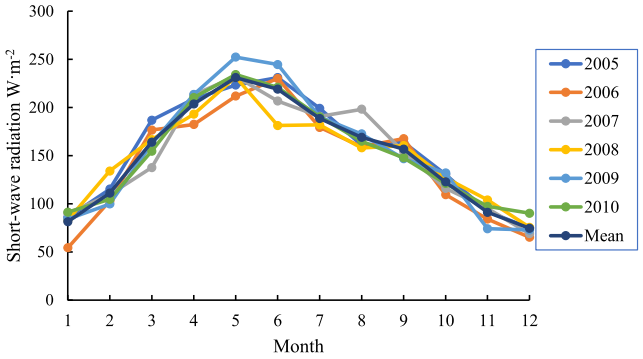

FIGURE 5. The mean daily shortwave radiation in the region.

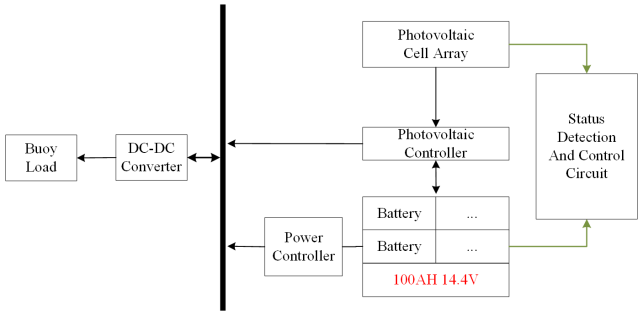

FIGURE 6. The architecture of the buoy power system.

batteries under bridge mode. The power controller is added to ensure an efficient balance of charge and discharge cycle of the batteries.

The effective management strategy of power supply could reduce the system consumption when it is not working or cut off the power supply of the internal working part at certain period or make it wait, which will effectively extend the battery life. According to all specifications of marine hydrological observation and minimum requirements of marine observation elements [19], we have chosen appropriate sensor and designed power control strategy to minimize the power assumption. In details, the lanterns and water quality monitoring sensors are both powered by their own internal battery packs. In addition, according to the requirements of observation, all sensors are categorized by their working time. It is specified that water quality monitoring sensors, ADCP, tide measurement module and wind monitoring sensor only work 12 minutes per hour, the visibility sensor only works 12 minutes per hour from 6 pm to 6 am the next day. The data acquisition and communication module work 24 hours per day. The specific allocation strategy can take full usage of the power supply as detailed in Table 2 and Table 3.

The battery capacity is another important factor affecting the batter performance. Generally, the discharge depth of the battery should be not more than 70%, and it should leave a margin for the system with regard to the influence of continuous rainy and windless weather. The system should alarm when the system energy storage is lower than 25%. When it is lower than 10%, the non-important loads should be unloaded automatically to ensure the power consumption for the data communication. Therefore, in good weather the solar

TABLE 2. The list of total power consumption for No.35 buoy.

Type of equipment/module	Voltage	Mean Current at 12V	Maximum mean power	Actual Power	Work strategy
Lantern (powered by internal battery packs)	3.8V	0.1A	1.2W	0.6W	12 hours at night (6 pm to 6 am the next day)
Visibility sensor	12-50 V DC	0.165A	1.98W	0.198W	12 hours at night (6 pm to 6 am the next day)
Water quality monitoring sensor (powered by internal battery packs)	10-24 V DC	0.042A	0.504W	0.1008W	12 hours at night (6 pm to 6 am the next day); 12 minutes per hour
GNSS OEM Board (including antennas)	12 V DC	1.18A	14.16W	2.832W	12 minutes per hour
ADCP	11-36 V DC	0.61A	7.32W	1.464W	12 minutes per hour
Data acquisition and control module	9-20 V DC	0.52A	6.24W	6.24W	24 hours
Communication module	9-20 V DC	0.26A	3.12W	3.12W	24 hours
Total power (Independent power supply equipment is not included)		2.735A	32.82W	13.855W	

TABLE 3. The list of total power consumption for No.40 buoy.

Type of equipment/module	Voltage	Mean Current at 12V	Maximum mean power	Actual Power	Work strategy
Lantern (powered by internal battery packs)	3.8V	0.1A	1.2W	0.6W	12 hours at night (6 pm to 6 am the next day)
Water quality monitoring sensor (powered by internal battery packs)	10-24 V DC	0.042A	0.504W	0.1008W	12 minutes per hour
ADCP	11-36 V DC	0.61A	7.32W	1.464W	12 minutes per hour
Wind monitoring sensor	8-30 V DC	0.005A	0.15W	0.03W	12 minutes per hour
Data acquisition and control module	9-20 V DC	0.52A	6.24W	6.24W	24 hours
Communication module	9-20 V DC	0.26A	3.12W	3.12W	24 hours
Total power (Independent power supply equipment is not included)		1.395 W	16.83W	10.854W	

panel and battery pack is used as the main and supplementary power supply, respectively. However, in extreme rainy weather, the battery can replace solar panel as the main power supply. All equipment voltage, except for the independent power supply component, is DC wide voltage with output 12V. Additionally, to avoid the adverse effect of buoy rotation on the conversion efficiency of solar energy, four solar panels are installed along four different directions. Taking No.35 buoy with higher power consumption as an example, the average power of the equipment at 12V DC is 13.855WH per day. Combined with the uncertain factors during the operation of the electric equipment, 24-hour power consumption of No.35 buoy is estimated as 28WH/1000=0.028 kWh. Assuming that there is no sunlight available for one month, a battery with capacity of 0.028 kWh∗30∗1000/12=70AH should be used to support normal function of the system [20]. Thus, a battery capacity of 100AH @14.4V could guarantee a minimum redundancy of 100AH∗14.4V/28WH≈51.4 day. Photovoltaic power should be considered as well. For each solar panel with size 1068mm x 806mm and square array is greater than or equal to 100 W/m^2, the power capacity of solar panel per day (6 hour) could be approximately estimated as 1.068m∗ 0.806m∗100W/m^2 ∗6h/1000 = 0.516 kWh. The effective working period with pure solar panel can be estimated as 0.516kW·h/0.028 kWh ≈18.4 day.

C. SENSORS

In order to understand water features water temperature, electrical conductivity, dissolved oxygen and chlorophyll-a are recorded with RBR concerto (https://rbr-global.com/products/standard-loggers/rbrduo-ct) in test region in test region. water quality monitoring equipment with a size of 490∗63.5mm, a solid-state memory of 128MB and default sampling rate with 1Hz, is included in the system. The sensor is fixed at instrument well (Table 4) and kept 20 cm away from the bottom of the buoy to avoid the organisms at the bottom of the buoy. To avoid uneven extrusion of external force on the instrument shell, the sensor is anchored with plastic clips or cotton ropes.

Retrieving flow information at a high spatial resolution is crucial for understanding the limno-physical boundary conditions [21], e.g., flow paths, currents, etc. RTI SeaPROFILER (https://rowetechinc.com/seaprofiler/) with 600kHz working frequency is used to record flow speed and direction in a profile from 1.5m below sea level to the seafloor with a cell size of 1m (Table 4 for detailed specifications). An ADCP is used to determine current velocities by using the Doppler shift of a backscattered acoustic signal [22]. The acoustic frequency of the ADCP is compromised by the desired vertical resolution and the water depth at the site [23], [24]. Here, the ADCP operates at a frequency of 600 kHz. The sensor has four 20° beam angles and 0.5m blanking distance. It offers a profiling range of 0m to 90 m, the maximum number of bins as 200 and the minimum cell size as 2cm. For the test deployment, 20 number of bins and 1m cell size are chosen. Considering the possible magnetic interference of iron physical objects, ADCP is installed more than 0.5m away from the physical objects.

To measure environmental features surrounding the buoy, it is important to obtain the meteorological information close to the water area surface. Thus, meteorological sensors are another indispensable part of the buoy monitoring system (Table 4). Wind speed and wind direction are recorded with a RM Young Wind Monitor 05106 (http://www.youngusa.com). Visibility sensors is chosen as VAISALA PWD50 (https://www.vaisala.com/en).

Tide information is normally collected by self-contained pressure tide gauge, float-type tide gauge and acoustic tide gauge, however they have poor real-time performance, high cost and large errors that prohibit their usage under the harsh marine environment [25]–[28]. Here tide information is recorded with K528 GNSS OEM board (http://www.sinognss.com/). K528 GNSS OEM Board is fixed in the freeboard cabin with waterproof, moisture-proof and salt fog-proof SS antenna and cables outside. A method based on Beidou difference location is adopted for tide monitoring as shown in Fig. 7.

$$H_t = (H_1 + H_2 + H_3 + H_4)/4 \quad (1)$$

$$\Delta H_w = H_t - \Delta H_{vAg} - H_w \quad (2)$$

TABLE 4. Allocation and technical overview of the sensors in the buoy monitoring system.

Type of Sensor	Parameter(Unit)	index	Location of Assembly
TYH-120 Lantren		LED built-in 100AH battery Running for 45 days without any solar charging 256 flash patterns with IR remote control	On the lantern guard
VAISALA PWD50 (Visibility sensor)	Visibility (m)	10m-35000m/ ± 10% of reading 10m-10000m, ±20 % of reading 10000m ~ 35000m	The upper bracket of No.35 buoy.
RBR concerto (C.T.D)	Water Temperature (℃)	-5℃-35℃/±0.002℃	No. 35 buoy. Evenly bound with plastic clips and cotton ropes and placed in the instrument well, and measuring position is 1m under water surface.
	Electrical Conductivity ($mScm^{-1}$)	0-85mS/cm/±0.003ms/cm (35psu 15°C)	
RBR concerto (DO.CDOM.Chla)	Dissolved Oxygen (mgL^{-1})	0-500μm (saturation 0-150%) maximum of ±8μm or ±5%	No. 40 buoy. The method is the same as above
	Chlorophyll-a (μgL^{-1})	0.02-150μgL^{-1}/±2%	
RTI SeaPROFILER (Acoustic Doppler Current Profiler)	Flow Speed (mms^{-1})	±5ms^{-1} (default), ±5ms^{-1} (maximum), long-term accuracy: ±0.25%, ±2mm/s 600kHz	No. 35 buoy. Install on the fixed bracket flange and place in the instrument well. 1.5m water depth with 0.5 m blanking distance and with measurement cell size of 1 m. resulting measurement range is from 2 to 21 m
	Flow Direction ($deg10^{-1}$)	0~360°/±1°	
RM Young 05106 (Winter Monitor)	Wind Speed (ms^{-1})	0~100ms^{-1}/ (±0.3ms^{-1} or 1% of measured value)	Install at the upper bracket of No.40 buoy.
	Wind Direction (deg)	0~360°/±3°	
K528 GNSS OEM Board	Attitude, Location	Signal tracking Channels:198 Post Processing Horizontal accuracy: ± (2.5 +1×10-6×D) mm Post Processing Vertical accuracy: ± (5 + 1×10-6×D) mm	GNSS antennas is more than 2m installed at the upper bracket of No.35 buoy and the OEM board is fixed in the freeboard cabin.

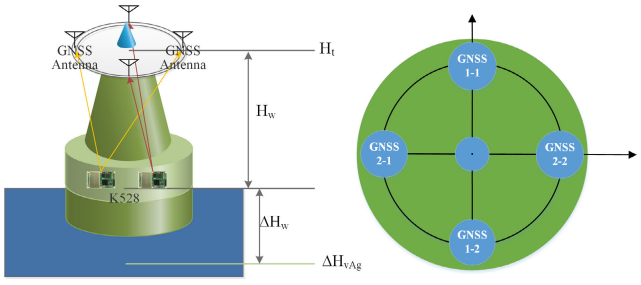

FIGURE 7. The principle of this method.

where ΔH_W is tide height, H_t represents instantaneous geodetic height of 4 antennas; ΔH_{vAg} represents geodetic height of the depth datum at Tianjin Port; H_W represents the height difference between the central geodetic height of the buoy waterline and the central geodetic height of 4 antennas. According to the installation position of 4 antennas, a dynamic model of the buoy could be established.

The coordinate and attitude data in standard NMEA protocol data is output from K528 GNSS OEM board via RS232 serial port. The real-time position and inclination of the buoy could be obtained based on the three-dimensional coordinates and attitude data uploaded by K528 GNSS OEM board.

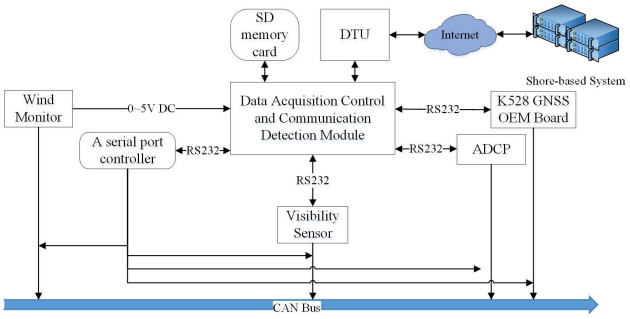

FIGURE 8. The structure of data acquisition and communication.

D. DATA ACQUISITION AND COMMUNICATION

In order to ensure the stability and reliability of the data acquisition and communication link, an independent module based on ARM is developed (Fig. 8). The data acquisition and control subsystem adopt master-slave dual redundancy protocol. Once the master system breaks down, the slave system can detect the error and put the system under control to ensure the reliability of system. Wireless communication mode is adopted for data transmission with the bandwidth rate not less than 64 KB/s and the effective data receiving rate is not less than 95%. The communication module could monitor and initialize equipment remotely to ensure the reliability of buoy monitoring system. All sub-modules related to master-slave dual redundancy module is connected together through CAN bus.

E. DESIGN OF SHORE-BASED ENVIRONMENTAL MONITORING SYSTEM

In order to monitor water area around the buoy system, a shore-based environmental monitoring system is developed based on J2EE software structure and multi-layer distributed application model. Acquired data could be processed in real time and displayed visually. The system mainly includes four modules: data management, comprehensive configuration, remote control management and data query. Data management module is composed of data storage, query, display, editing and maintenance (Fig. 9a). Comprehensive configuration module includes the configuration of control module and sensors for buoy monitoring system (Fig. 9b). Control management module could obtain remotely the operation status of different sensors, and set up sensor's initialization, acquisition interval, working time range, etc. Data query module provides retrieval function of historical data, system log, and equipment relationship. The system has been previously applied in Tianjin Hydrographic Science & Technology Center [29].

III. FIELD EXPERIMENT

Many ships have been passing through the dual channel at Tianjin port, which brings difficulties to the real-time hydrological monitoring test. The buoy monitoring system was deployed near the breakwater gate of Tianjin Port in July 2016, The coordinates of No.35 buoy are

FIGURE 9. Shore-based environmental monitoring system. (a)Real-time monitoring information and data management module; (b) Comprehensive configuration module.

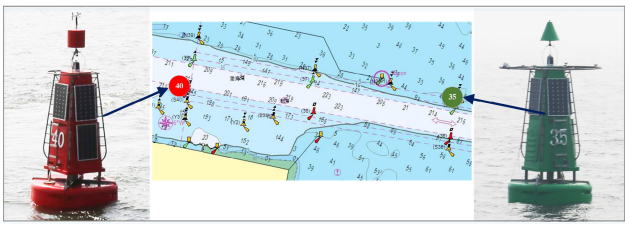

FIGURE 10. Map of test deployment of monitoring system.

$117°54'56''E$, $38°57'13''N$, and those of No.40 buoy are $117°51'58''E$, $38°57'22''N$ as shown in Fig. 10.

The buoy platform had been treated with biological anti fouling coating to prevent the attachment of marine organisms. In the following part, unless otherwise states, continuous monitoring data from November 1st to November 30th, 2016 at Tianjin port is used for data analysis while ADCP data is collected from November 8th to December 9th due to shortage of power energy.

IV. RESULTS AND DISCUSSION

A. WATER QUALITY ANALYSIS

Water quality data include time variations of water temperature, salinity and electrical conductivity on No.35 buoy (Table 4) and time evolution of dissolved oxygen and chlorophyll-a on No.40 buoy are collected by RBR concerto on each buoy. Fig. 11(a), (c) and (e) shows the time evolution of temperature, salinity and electrical conductivity during the test period. The daily mean time evolution of the above-mentioned factors could be gotten from Fig. 11(b), (d) and (f), respectively. During the test period, the temperature varied from 5.5 °C to 13.6 °C, and the maximum daily temperature reaches 12.9 °C on November 3rd. As for electrical conductivity, it changes from 0.28 mS/cm to 0.35 mS/cm with a maximum value of 0.34 MS/cm on November 5th. Similar to the temperature, the electrical conductivity homogenizes with regard to the water depth within the observation period. On contrary, the time evolution of salinity shows a unregular trend due to the intercoupling of multiple factors. However, the evolution range of salinity keeps consistent with previous results in winter.

Fig. 12 (a) and (b) shows daily and monthly evolution of dissolved oxygen. The dissolved oxygen concentration change from 7.54 mg/L ∼8.84mg/L, and the daily mean value reached to maximum of 8.36mg/L on November 1st. During the test period, the dissolved oxygen concentration conforms well to the class I water quality standard of sea water (>=6mg/L) [30]. The dissolved oxygen concentration at the monitoring water area is relatively stable. The dissolved oxygen concentration decreases for half a month and increased slightly at the end of the month.

Chlorophyll-a is the one important pigment in phytoplankton as its concentration is not only a sign of phytoplankton quantity, but also an important indicator of marine environment [31]. From Fig. 12 (c) and (d), the evolution profile of chlorophyll-a concentration is similar to that of dissolved oxygen, but the concentration is relatively low during the test period. The maximum of chlorophyll-a concentration reached to 1.4ug/L on November 1st. The chlorophyll-a concentration may be affected by the temperature, terrestrial input, wind speed, tide and other factors. From Fig. 11 (a) (referring to the temperature monitoring of No. 35 buoy), the temperature gradually decreases resulting in the slow growth of the marine phytoplankton. In addition, the seasonal variation of sea surface temperature will cause the stratification or mixing of water body, and then affect the seasonal distribution of chlorophyll-a concentration. The Chlorophyll-a concentration at Tianjin port is consistent with the previous studies in the Bohai Sea in the winter season [32].

Apart from temperature, we guess that wind stress is another important factor contributing to the variability of phytoplankton growth. Previous studies have shown that wind condition will influence the chlorophyll-a concentration through the seasonal variability of wind mixing [33]. Fu yanhao *et al* have found similar trend of chlorophyll-a concentration in the Bohai Sea and proposed positive correlation between chlorophyll-a concentration and wind speed in summer and autumn offshore, and negative correlation in winter near the coast [34]. The negative correlation between wind speed and chlorophyll-a concentration, suggested that wind speed will restrict the phytoplankton growth. This may be because the wind speed promotes the full exchange between the surface layer and the bottom layer of seawater and brings nutrients to the surface layer. When the ratio of nitrogen to phosphorus and the ratio of silicon to nitrogen in nutrients exceeds over or falls below a certain threshold, the growth, reproduction and chlorophyll-a

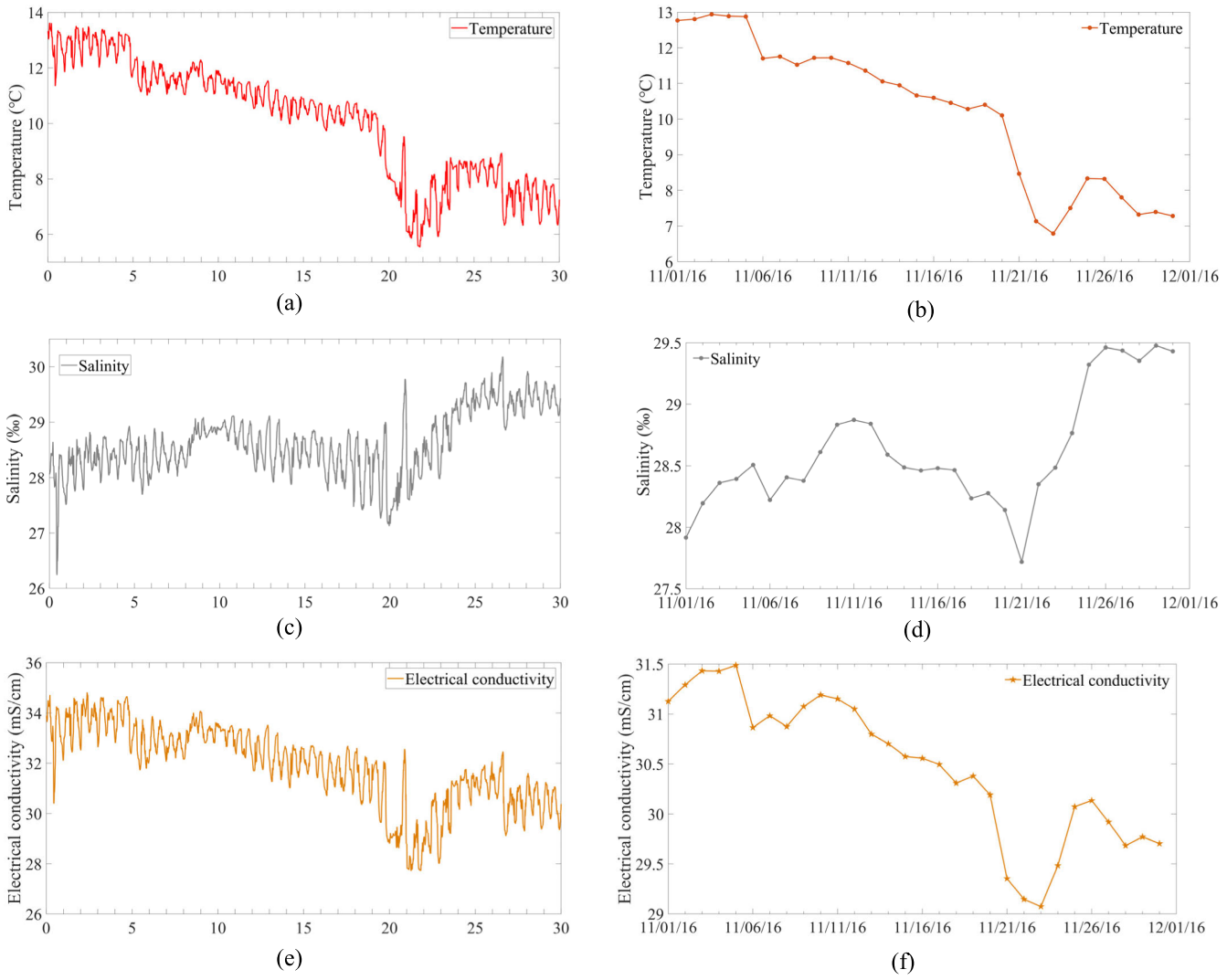

FIGURE 11. Water quality monitoring factors recorded by RBR concerto at No.35 buoy. (a) Time evolution of temperature; (b) The daily mean time series of temperature; (c) Time evolution of salinity; (d) The daily mean time series of salinity; (e) Time evolution of electrical conductivity; (f) The daily mean time series of electrical conductivity.

concentration distribution of phytoplankton will be inhibited [35]. Moreover, the wind would probably reduce the resistance time of phytoplankton in the euphotic layer, thus decrease the biomass in the surface layer. However, this correlation is not apparent, which might be attributed to the wind speed in the monitoring period is not strong. When the wind speed increases, it would enhance the material exchange between different sea water level, and then might affect the chlorophyll-a concentration.

Terrestrial input is another an important factor affecting the chlorophyll-a concentration near the shore. Bohai Sea is the largest inland sea in China, with more than 40 rivers flowing in. The runoff brings a large amount of nutrients into the estuarine coastal waters, which intensifies the eutrophication of the water. Zhang *et al.* have shown that the increase of nutrient input from rivers in 2000-2012 made chlorophyll-a concentration increasing in the Bohai Sea [36].

Regarding to the dissolved oxygen concentration, there is a significantly positive correlation between chlorophyll-a concentration and dissolved oxygen concentration. Phytoplankton can absorb carbon dioxide and release oxygen through photosynthesis, which results in the increase of dissolved oxygen concentration in the surface layer. The positive correlation could be beneficial to environmental monitoring like red tide warning which make the dissolved oxygen concentration as indirect measurement factor to estimate the proper chlorophyll-a concentration.

B. METEOROLOGICAL ANALYSIS

Fig. 13 shows the visibility recorded by the No.35 buoy. The visibility monitoring set two different data acquisition frequencies of 1 min and 10 min. The range of visibility changed from 50 m to 35000 m. Combined with the PM2.5 concentration and related meteorological data, Li *et al.* have analyzed the variational characteristics and influencing factors of atmospheric visibility over 2013-2016 in Tianjin urban area by using the MODLE6000 forward-scattering visibility meter produced by Yinghua *et al.* [37]. Their results showed that

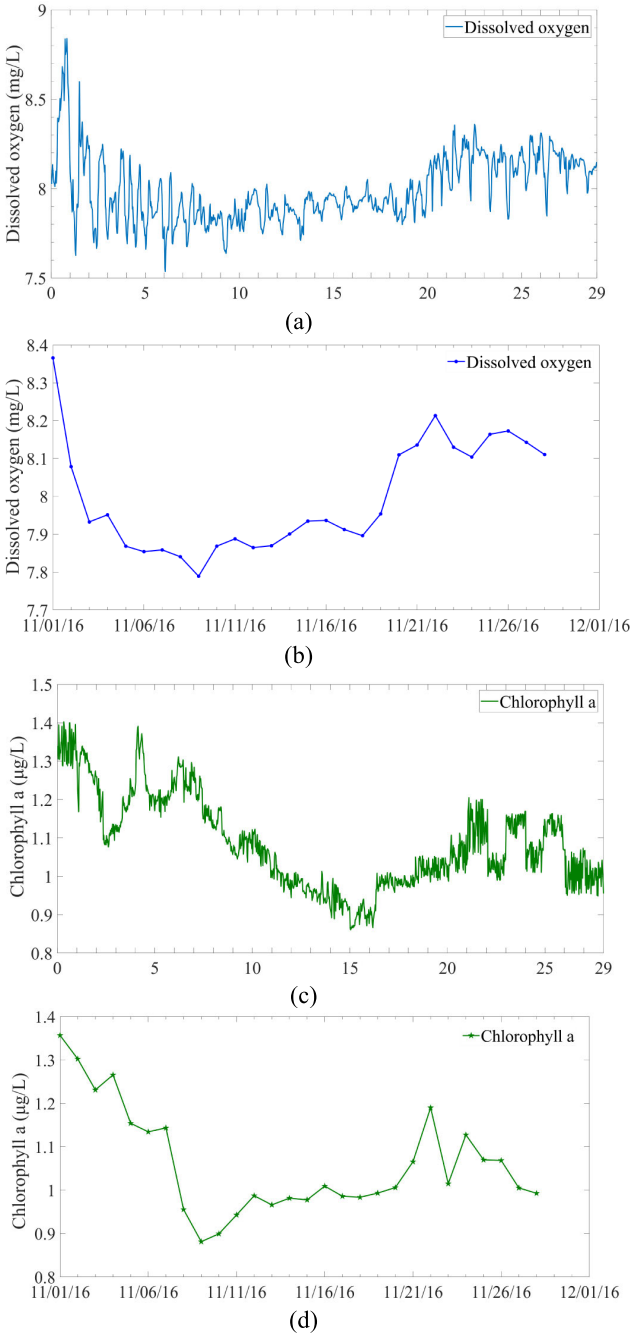

FIGURE 12. Water quality monitoring factors recorded by RBR concerto at No.40 buoy. (a) Time series of dissolved oxygen concentration; (b) The daily mean time series of dissolved oxygen concentration; (c) Time series of chlorophyll-a concentration; (d) The daily mean time series of chlorophyll-a concentration.

the average atmospheric visibility was 11.23 km during the measurement period; The visibility features have analyzed using automatic hourly visibility observations at Tianjin Port from 2009 to 2013 by Wu Bingui etc [38]. Similar visibility features prove the rationality of our measured results.

Wind speed and direction are plotted in a wind rose diagram as shown in Fig. 14. The test region prevailed south and southeast wind during the test period with a wind direction

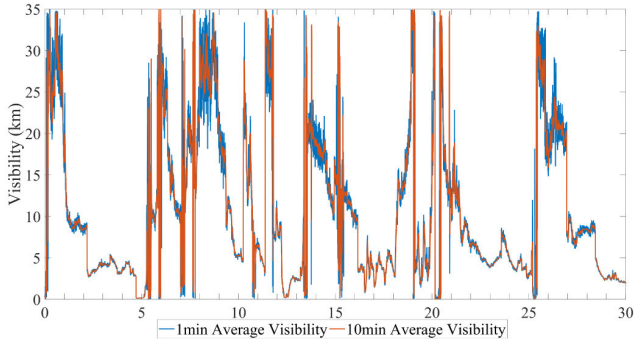

FIGURE 13. Visibility recorded by visibility sensor at No.35 buoy.

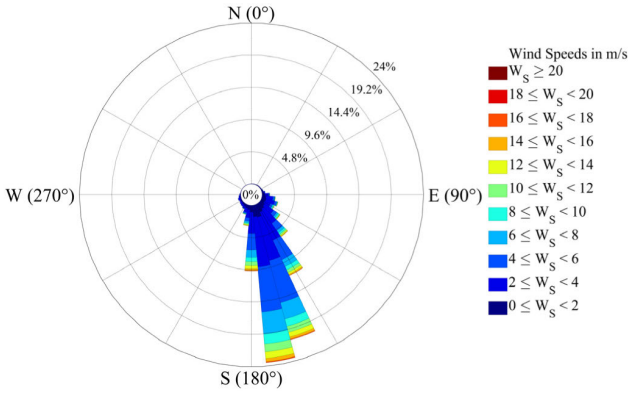

FIGURE 14. Wind Speed and wind directions recorded by wind monitoring.

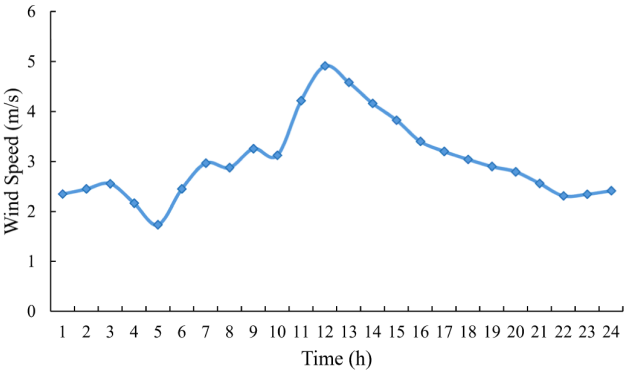

FIGURE 15. Distribution probability of wind speed at all levels during the test periods.

concentrated between 150° and 180°. The mean wind speed reached 4.0 m/s, even reaching to the climax as 20m/s on November 21st with a certain direction of 176°. To verify our test, data from Tang Gu meteorological station (16.4km away from the test site) shows that the monthly average wind speed of test site (http://data.sheshiyuanyi.com/weatherdata/) in November 2016 is 2.4m/s, which agrees well with measured wind speed at the test site. Indeed, the wind speed on the water body is generally higher than that forecasted by the weather station because the atmospheric stratification on the water body is unstable, and the air temperature is relatively high on the sea that results in stronger turbulent exchange

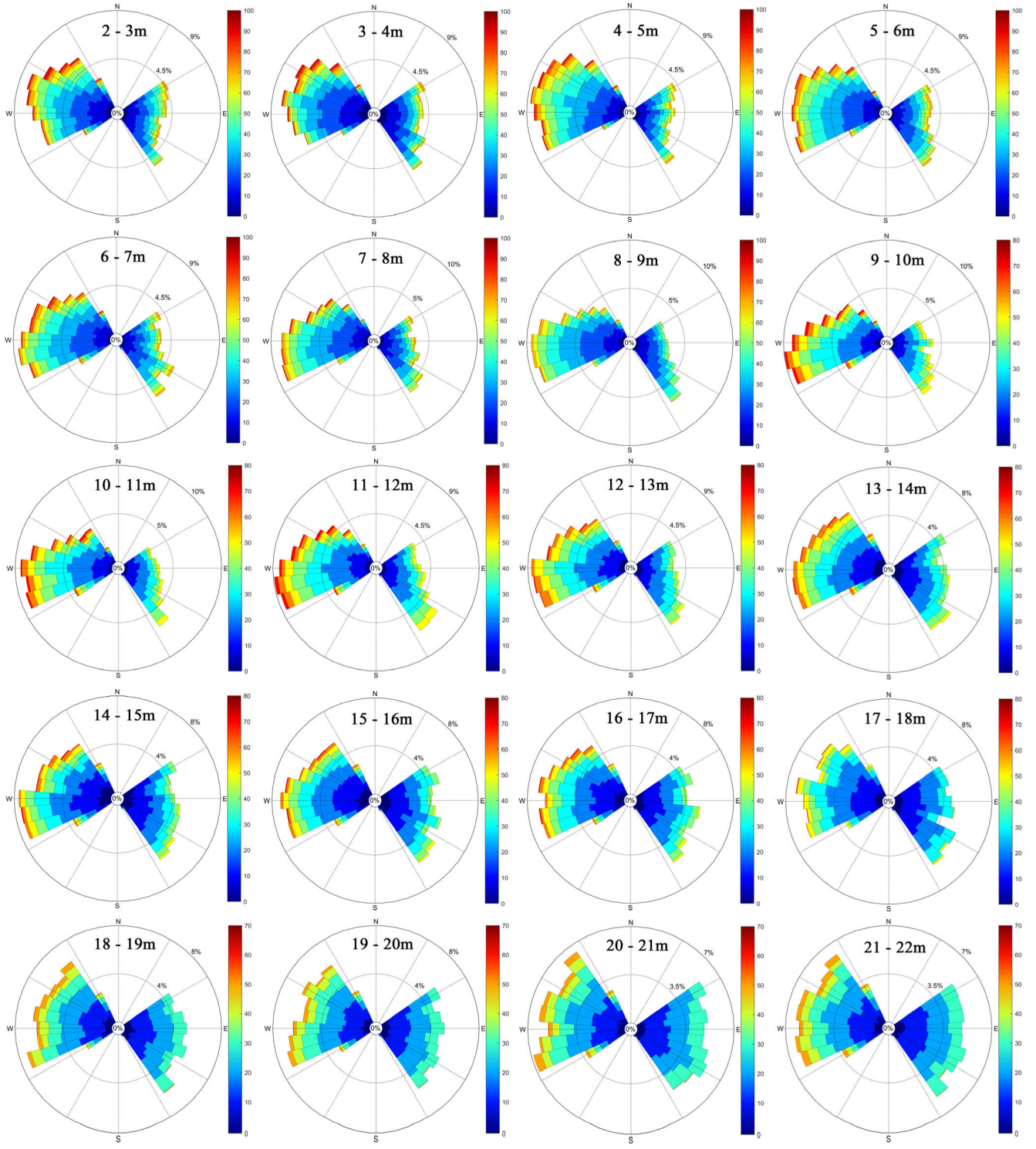

FIGURE 16. Flow speed and directions over all depths per cardinal direction recorded by ADCP.

than that on the land, which will strengthen the wind speed on bottom layer of water body. Additionally, the increment of wind speed caused by the smoothness of the water surface is greater than that caused by the change of the stratification stability, to make wind speed above water body slightly larger than that on land. Our observation basically conforms to this intuitive physical law.

Fig. 15 shows that the coastal near surface wind speed is affected by both the ocean and the land at the same time. Taking the data on November 2nd as example, the wind speed is relatively stable before sunrise, then with the increment of time, the wind speed reaches to the maximum around two o'clock in the afternoon, then the wind speed gradually weakens. The reason for this interesting phenomenon can

be attributed to the strong turbulence of the heated ground after sunrise. This intense thermal exchange makes kinetic energy transport from upper to lower layer, which resulted into higher speed in the daytime with the largest kinetic energy transmission. However, the ground radiation gradually weakens after sunset, the atmosphere tended to be stable and the wind speed gradually decreases.

C. CURRENT ANALYSIS

In order to analyze the tide characteristics of Tianjin port, current data is monitored during the test period. We obtain the flow speed and flow direction during the test period by smoothing the current data which have been eliminated the large error and filtered [39]–[42]. Fig. 16 shows the rose chart of flow speed and direction measured by ADCP in different depths and layers. The tidal current at Tianjin Port has apparent reciprocating characteristics. From the surface tidal current, the flood flow velocity is slightly higher than that of ebb tide. The maximum flood flow velocity of the surface layer reaches 99.60cm/s, while the maximum ebb flow velocity is 79.55cm/s. The angle between the average tidal current direction and the main channel (281°−101°) direction is about 20°, and the main flow along WNW-ESE direction roughly follows along the bathymetric contour during the test period as shown in Fig. 10. In the vertical direction, the flood mean flow velocity of the surface (2-3m), middle (10-11m) and bottom (21-22m) layers reaches to 35.24cm/s, 32.83cm/s and 25.99cm/s, respectively, and the ebb mean flow velocity of the surface (2-3m), middle (10-11m) and bottom (21-22m) layers reaches to 30.83cm/s, 27.31cm/s and 21.51cm/s, respectively. It agrees with the fact that the velocity of flood tide is greater than that of ebb tide. The overall velocity is not large that belongs to the weak- current sea area. With the increment of the depth, the mean velocity decreases gradually and attains a minimum near the bottom due to the energy loss from the friction of the sea bottom. The variation time of flow speed and direction in each layer kept similar which indicated that there was no obvious vertical stratification phenomenon of current flow in this area.

V. CONCLUSION

An innovative multifunctional buoy monitoring system assembled with many kinds of perception equipment is introduced for continuous monitoring port environmental dynamics. The combination of battery module and solar power supply mode could realize observation without interruption. And through wireless communication, the acquired data were achieved the transmits to the shore-based environmental monitoring system in real-time mode. What's more, shore-based monitoring system was designed for further data analysis that provides technical support for follow-up forecast. Through combining theoretical and long-term experimental deployment, we verify the effective of the mooring buoy system for port environmental dynamics observation. As all measurement units, power supply and data transfer functioned without failure and with data ranges that were in the order of magnitude of consistent observations in other studies.

Compared to the traditional observation buoy, the system set up instrument wells that ensures convenient installation and safety of the sensor units. Especially, all sensor units could be achieved maximum maintainability due to easy accessibility. In addition, the system enhances the energy supply with battery module and solar power supply. This method enhances the load capacity of the buoy, so that it can satisfy the requirement of carrying more sensors and communication equipment. This system designs an independent module based on ARM to ensure the stability and reliability of the data acquisition and communication link. Furthermore, a method of tide measurement based on Beidou difference for buoy platform was proposed, which was proved to be an effective method for tide measurement. And a shore-based monitoring system was developed for real-time display and data analysis.

Based on the observation data, on the one hand, the effectiveness and reliability of the designed buoy observation system were proved. On the other hand, the hydrological environmental characteristics of Tianjin port water area were analyzed in this study. The water quality monitoring results of No.35 buoy reflected that temperature, wind speed and terrestrial input also became the key factors affecting the evolution of dissolved oxygen and chlorophyll-a concentration. As for current data, we analyzed the current characteristics of Tianjin port, and found that the sea area presented obvious reciprocating characteristics, the overall velocity is not large, which belongs to the weak-current sea area, and there was no obvious vertical stratification phenomenon. Finally, the meteorological data was revealed, and the time series characteristics and influencing factors of visibility, wind speed and wind direction were excavated, respectively.

Recorded data clearly showed water area characteristics of Tianjin Port with the test deployment period. However, it should be paid more attention to the more sensor's units and further data analysis. The first problem is the limitation of observation time and observation area, our analysis mainly verified the reliability and effectiveness of the designed buoy observation system in Bohai Sea. Nevertheless, short-term observation period could not fully characterize the temporal and spatial characteristics of the observation area, only long-term observation accumulation could reach this goal. This is also the focus of our next task based on our own design platform. In addition, there are some design defects in the process of observation. For example, ADCP could apply for flow velocity from 2m underwater to the bottom, and we could not obtain the surface velocity exactly. One reliable strategy pursued is to obtain surface flow velocity information by using the Current Meter. Thus, maximum spatial coverage and resolution could be achieved through highly resolved flow velocity measurement by two sensors. Besides, communication and data transmission ability should further be developing with integrating Beidou, 5G, acoustic, and AIS communication, to realize the real-time communication for ocean three-dimensional observation. Moreover, in the future, we plan to carry high-precision MEMS mechanical sensor to

obtained attitude information of buoy, then combined with the motion law of buoy and interaction with the environment, we could calculate the trajectory of wave and current through the comprehensive analysis and processing.

In summary, it can be stated that the buoy system presented here is a very valuable tool for continuously measuring port environmental dynamics. The buoy will find it marine applications and contributes to the coastal ocean observing system.

ACKNOWLEDGMENT

This work has been carried out in the frame of the Tianjin Port e-Navigation Project. The data set of solar radiation is provided by the National Tibetan Plateau Data Center.

REFERENCES

[1] Y. Liu, H. Kerkering, and R. H. Weisberg, *Introduction to Coastal Ocean Observing Systems, Coastal Ocean Observing Systems*, Y. Liu, Ed. New York, NY, USA: Academic, 2015, pp. 1–10.

[2] E. Canepa, S. Pensieri, R. Bozzano, M. Faimali, P. Traverso, and L. Cavaleri, "The ODAS italia 1 buoy: More than forty years of activity in the ligurian sea," *Prog. Oceanogr.*, vol. 135, pp. 48–63, Jun. 2015, doi: 10.1016/j.pocean.2015.04.005.

[3] Y. Liu, R. H. Weisberg, C. R. Merz, S. Lichtenwalner, and G. J. Kirkpatrick, "HF radar performance in a low-energy environment: CODAR SeaSonde experience on the west florida Shelf*," *J. Atmos. Ocean. Technol.*, vol. 27, no. 10, pp. 1689–1710, Oct. 2010, doi: 10.1175/2010JTECHO720.1.

[4] M. H. Freilich and R. S. Dunbar, "The accuracy of the NSCAT 1 vector winds: Comparisons with national data buoy center buoys," *J. Geophys. Res., Oceans*, vol. 104, no. C5, pp. 11231–11246, May 1999.

[5] C. A. K. MearsD Smith and F. J. Wentz, "Comparison of SSM/I and buoy-measured wind speeds from 1987 to 1997," *J. Geophys. Res.-Oceans*, vol. 106, no. C6, pp. 11719–11729, 2001.

[6] G. Novelli, C. M. Guigand, C. Cousin, E. H. Ryan, N. J. M. Laxague, H. Dai, B. K. Haus, and T. M. Özgökmen, "A biodegradable surface drifter for ocean sampling on a massive scale," *J. Atmos. Ocean. Technol.*, vol. 34, no. 11, pp. 17–55, 2017, doi: 10.1175/JTECH-D-17-0055.1.

[7] R. Venkatesan, G. Vengatesan, N. Vedachalam, M. A. Muthiah, R. Lavanya, and M. A. Atmanand, "Reliability assessment and integrity management of data buoy instruments used for monitoring the indian seas," *Appl. Ocean Res.*, vol. 54, pp. 1–11, Jan. 2016, doi: 10.1016/j.apor.2015.10.004.

[8] R. Cole, R. Weisberg, J. Donovan, C. Merz, R. Russell, V. Subramanian, and M. Luther, "The evolution of a coastal mooring system: A simple current meter mooring is transformed into a complete 'Air-Sea Interaction' monitoring system in the Gulf in Mexico," *Sea Technol.*, vol. 44, no. 2, pp. 24–31, 2003.

[9] J. P. Wallinga, N. R. Pettirew, and J. D. Irish, "The GoMOOS moored buoy design," in *Proc. Oceans Celebrating Teaming Toward Future*, Sep. 2003, pp. 2596–2599.

[10] C.-C. Teng, L. Bernard, B. Taft, and M. Burdette, "A compact wave and ocean data buoy system," in *Proc. OCEANS MTS/IEEE*, Sep. 2005, pp. 1249–1254.

[11] T. Nagai and K. Shimizu, "Basic design of Japanese nationwide GPS buoy network with multi-purpose offshore observation system," *J. Earthq. Tsunami*, vol. 3, no. 2, pp. 113–119, Jun. 2009, doi: 10.1142/S1793431109000494.

[12] S. Pensieri, R. Bozzano, M. E. Schiano, E. Canepa, P. Picco, and L. Pensieri, "The W1-M3A multidisciplinary off-shore observing system," in *Proc. MTS/IEEE OCEANS Bergen*, Jun. 2013, pp. 1–9.

[13] R.H. WeisbergL. Zheng and Y. Liu, *Basic Tenets for Coastal Ocean Ecosystems Monitoring, Coastal Ocean Observing Systems*, New York, NY, USA: Academic, 2015, pp. 40–57.

[14] J. Wang, Z. Wang, Y. Wang, S. Liu, and Y. Li, "Current situation and trend of marine data buoy and monitoring network technology of China," *Acta Oceanologica Sinica*, vol. 35, no. 2, pp. 1–10, Feb. 2016, doi: 10.1007/s13131-016-0815-z.

[15] Wikipedia. (2020). *Bohai Sea*. [Online]. Available: https://en.wikipedia.org/wiki/Bohai_Sea

[16] (Sep. 2020). *L. Shanghai BOYUN Supply Chain Management Co*. Tianjin Port. [Online]. Available: http://www.chinaports.com/ports/7a40cab9-3b4e-4060-bc66-79e0977d47b7

[17] T. Tomisa, S. Krajcar, and D. Pinezic, "Multipurpose marine Buoy," in *Proc. 50th Int. Symp. ELMAR*, Zadar, Croatia, 2008, pp. 401–405.

[18] T. Wenjun, "Daily average solar radiation dataset of 716 weather stations in China (1961–2010)," Nat. Tibetan Plateau Data Center, ITP-CAS, Beijing, China, Tech. Rep., 2018, doi: 10.11888/AtmosphericPhysics.tpe.249399.file.

[19] *Specifications for Oceanographic Survey—Part 2: Marine Hydrographic Observation, Book Specifications for Oceanographic Survey—Part 2: Marine Hydrographic Observation, Series Specifications for Oceanographic Survey—Part 2: Marine Hydrographic Observation*, SOA, New Delhi, India 2008.

[20] C.-C. Lee and S.-H. Park, "Different approaches to design a meteorological buoy for weather monitoring purposes," *J. Inf. Commun. Converg. Eng.*, vol. 8, no. 3, pp. 301–306, Jun. 2010.

[21] P. Mueller, H. Thoss, L. Kaempf, and A. Güntner, "A buoy for continuous monitoring of suspended sediment dynamics," *Sensors*, vol. 13, no. 10, pp. 13779–13801, Oct. 2013, doi: 10.3390/s131013779.

[22] G. P. Holdaway, P. D. Thorne, D. Flatt, S. E. Jones, and D. Prandle, "Comparison between ADCP and transmissometer measurements of suspended sediment concentration," *Cont. Shelf Res.*, vol. 19, no. 3, pp. 421–441, 1999, doi: 10.1016/S0278-4343(98)00097-1.

[23] X. WenxiY Jinkun and Z. Xin, "Indentification and Correction of Layer Depth and Water Depth Data Measured by ADCP," *Mar. Sci. Bull.*, vol. 31, no. 01, pp. 94–96, 2012.

[24] F. Jianjun, "Principles of ADCP and methods of data processing," *Port Eng. Technol.*, vol. 1, no. 3, pp. 53–55, 2007.

[25] L. Guanwei and W. Wenbo, "Application of pressure tide gauge in waterway bathmetry," *Port Waterway Eng.*, vol. 1, no. z2, pp. 1–5, 2019.

[26] Y. Shukai, L. Hui, T. Yongzuo, L. Chengjie, Z. Wei and S. Lei, "Comparisons for float-type, pressure and radar tide gauge," *Inf. Technol. Informatization*, vol. 1, no. 3, pp. 132–134, 2019.

[27] L. Mingzhao and T. Rui, "Indication correction of acoustic tide gauge under uneven temperature conditions," *Ocean Technol.*, vol. 18, no. 2, pp. 69–73, 1999.

[28] W. Kunfa and H. Zhimin, "Application of pressure tide gauge in marine surveying and mapping," *Sci. Technol. Inf.*, vol. 16, no. 17, pp. 33–34, 2018, doi: 10.16661/j.cnki.1672-3791.2018.17.033.

[29] (Oct. 5, 2017). *Shore-Based Environmental Monitoring System*. [Online]. Available: 218.69.111.107:8081/enav/web/enav/web/newContent/index.jsp

[30] Z. Qiufeng, *Marine Ecosystem Health Assessment and Analysis of Tianjin Coastal Marine Areas*. Qingdao, China: Ocean Univ. China, 2006.

[31] K. Kallio, S. Koponen, and J. Pulliainen, "Feasibility of airborne imaging spectrometry for lake monitoring—A case study of spatial chlorophyll a distribution in two meso-eutrophic lakes," *Int. J. Remote Sens.*, vol. 24, no. 19, pp. 3771–3790, Jan. 2003.

[32] Z. Q. Xinhua and H. Guikun, "Analysis of the sediment chlorophyll distribution at tianjin coast," *J. Tianjin Univ. Sci. Technol.*, vol. 25, no. 6, pp. 18–21, 2010.

[33] I. N. Radiarta and S.-I. Saitoh, "Satellite-derived measurements of spatial and temporal chlorophyll—A variability in funka bay, southwestern hokkaido, japan," *Estuarine, Coastal Shelf Sci.*, vol. 79, no. 3, pp. 400–408, Sep. 2008, doi: 10.1016/j.ecss.2008.04.017.

[34] Y. Fu, S. Xu, and J. Liu, "Temporal-spatial variations and developing trends of Chlorophyll–A in the bohai sea, China," *Estuarine, Coastal Shelf Sci.*, vol. 173, pp. 49–56, May 2016, doi: 10.1016/j.ecss.2016.02.016.

[35] A. C. Redfield, "The influence of organisms on the composition of seawater," in *Book The Influence of Organisms on the Composition of Seawater* (Series The Influence of Organisms on the Composition of Seawater), 2th ed. Geneva, Switzerland: Interscience Publishers, 1963, pp. 26–77.

[36] Z. He and Z. Xiaoshen, "Study on red tide remote sensing monitoring in the Bohai Sea in 2014," *Mar. Sci. Bull.*, vol. 19, no. 1, pp. 37–51, 2017.

[37] L. Yinghua, Y. Liying, Y. Qing, H. Suqin, C. Ziying, and L. Jingle, "Analysis of variation characteristics and influencing factors of atmospheric visibility in Tianjin urban area from 2013 to 2016," *J. Environ. Eng. Technol.*, vol. 8, no. 4, pp. 349–358, 2018, doi: 10.3969j.issn.1674-991X.2018.04.046.

[38] W. Bingui, Z. Jianchun, L. Yinghua, W. Yanan, and X. Mei, "Research on numerical interpretative forecast for low-visibility at Tianjin Port in autumn and winter," *Meteorol. Monthly*, vol. 43, no. 7, pp. 863–871, 2017.

[39] Z. Anmin, N. Yiwei, W. Chenxu, Z. Hao, L. Rongxia, and S. Chaohui, "Study on the characteristics of tidal and residual currents of characteristics observation station in Tianjin Port main channel," *J. Mar. Sci.*, vol. 37, no. 1, pp. 75–82, 2019.
[40] C. Huang, K. Yang, H. Li, and Y. Zhang, "The flow noise calculation for an axisymmetric body in a complex underwater environment," *J. Mar. Sci. Eng.*, vol. 7, no. 9, p. 323, Sep. 2019, doi: 10.3390/jmse7090323.
[41] P. Schuchert, L. Kregting, D. Pritchard, G. Savidge, and B. Elsäßer, "Using coupled hydrodynamic biogeochemical models to predict the effects of tidal turbine arrays on phytoplankton dynamics," *J. Mar. Sci. Eng.*, vol. 6, no. 2, p. 58, May 2018, doi: 10.3390/jmse6020058.
[42] Z. Li, "Velocity profile data processing and error control in ADCP," M.S. thesis, Dept. Inf. Sci. Eng., Southeast Univ., Nanjing, China, 2015.

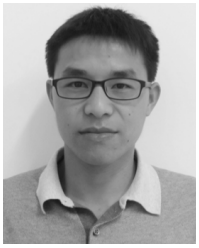

HAO ZHANG was born in Zhengzhou, Henan, China, in 1990. He received the M.S. degree in instruments science and technology from Shandong University, in 2017. He is currently pursuing the Ph.D. degree with the School of Marine Science and Technology, Tianjin University.

His research interests include e-navigation and marine data integration.

DIANJUN ZHANG was born in Shandong, China, in 1986. He received the M.S. degree from Beijing Forestry University, in 2011, and the Ph.D. degree from the Institute of Geographic Sciences and Natural Resources Research, Chinese Academy of Sciences, China, in 2015, all in geographical information system.

His research interests include optical remote sensing and ship recognition based on deep learning methods.

ANMIN ZHANG was born in Anhui, China, in 1966. He received the Ph.D. degree in photogrammetry and remote sensing from Wuhan University, in 2013.

From 2005 to 2014, he was an Outstanding Senior Engineer with the Beihai Navigational Security Center's Tianjin Marine Survey and Charting Center, Tianjin, China. He is currently a Professor, the Ph.D. Tutor, and the School Head of the School of Marine Science and Technology, Tianjin University. His research interests include e-navigation, marine geodesy and cartography, GIS, and unmanned underwater vehicle.